広島大学学術情報リポジトリ
Hiroshima University Institutional Repository

Title	New 3-D flow interpolation method on moving ADCP data
Auther(s)	Tsubaki, Ryota; Kawahara, Yoshihisa; Muto, Yasunori; Fujita, Ichiro
Citation	Water Resources Research , 48 (5)
Issue Date	2012
DOI	10.1029/2011WR010867
Self DOI	
URL	http://ir.lib.hiroshima-u.ac.jp/00034914
Right	Copyright 2012 American Geophysical Union. All Rights Reserved.
Relation	

New 3-D flow interpolation method on moving ADCP data

R. Tsubaki[1], Y. Kawahara[1], Y. Muto[2], and I. Fujita[3]

Abstract. A simple but accurate interpolation procedure for obtaining the three-dimensional distribution of three-component velocity data, from moving acoustic Doppler current profiler (ADCP) observation data, is proposed. For understanding actual flow structure within a river with complex bathymetry, the three-dimensional mean velocity field provides a basic picture of the flow. For obtaining the three-dimensional distribution of three-component velocity data, in this work, anisotropic gridding was introduced in order to remove the random component of measured velocity data caused by the turbulence of the flow and measurement error. A continuity correction based on the pressure equation was used to reduce both random and systematic errors. The accuracy of the developed method was evaluated using three-dimensional flow simulation data from a detached-eddy simulation (DES). By using the procedure developed, the complex flow structure surrounding the spur-dikes section in the Uji River was successfully visualized and explored. The proposed method shows superiorities in both accuracy and consistency for the interpolated velocity field, as compared to the Kriging and Inverse-Distance Weighted (IDW) methods.

1. Introduction

Riverine flow has an unambiguous streamwise direction, and this is a distinguishable feature from oceanic flow. Stream direction is restricted by geologic conditions and interacts with morphological changes within a river bed. As a result, riverine flow is significantly anisotropic. Coastal flows also have strong anisotropy. However, due to differences in morphological and fluid-dynamic conditions, flow structures within coastal and oceanic areas differ greatly from rivers.

An acoustic Doppler current profiler (ADCP) is useful for measuring water current velocities at various water depths. For river flow measurements, the time-series velocity, measured using a fixed ADCP survey, displays certain amounts of variation. The variation is due to random components that are caused by the turbulence of the flow (see e.g., *Muste et al.* [2004a]; *Stone and Hotchkiss* [2007]) and the random error of ADCP measurements (e.g., *Muste et al.* [2004b]; *Fugate and Chant* [2005]). In addition to the random errors of measurements, ADCP results contain systematic errors that are caused by the measurement system and the nature of riverine flow (e.g., *Joyce* [1989]; *Pollard and Read* [1989]; *Kaneko and Ito* [1994]; *Callede et al.* [2000]; *Ishii* [2006]). In fact, the anisotropy of flow motion and the unstableness of water surface and river bed induces strong systematic errors and greatly limits the accuracy of measured data. Therefore, a reasonable data process scheme for ADCP surveys in rivers should be established. In designing this scheme, one must consider river flow features and how sources of error impact measurements (e.g., *Ohmori et al.* [1997]; *Dinehart and Burau* [2005b]; *Nystrom et al.* [2002]; *Dinehart and Burau* [2005a]; *Muto and Baba* [2008]). An advantage of ADCPs is their ability to measure three-dimensional flow. From a scientific and practical standpoint, understanding three-dimensional flow structure is very important (e.g. *Blanckaert and Vriend* [2004]; *Constantinescu et al.* [2011]).

[1]Department of Civil and Environmental Engineering, Hiroshima University, Higashi-hiroshima, Japan.

[2]Department of Civil and Environmental Engineering, University of Tokushima, Tokushima, Japan.

[3]Department of Civil Engineering, Kobe University, Kobe, Japan.

For understanding flow structure within a river section with complex bathymetry, cross-sectional distributions provide limited insights. By using an accurate three-dimensional distribution of the mean velocity components, a comprehensive discussion of flow structure using complex geometry can be more easily accomplished (e.g., *Dinehart* [2003]; *Tsubaki and Fujita* [2007]). Furthermore, since measurements from a specific cross-section are not sufficient for understanding the full structure of a flow with complex geometry (*Jamieson et al.* [2011]), a singular cross-sectional plane is not adequate for flow over complex bathymetries. In this study, a simple but accurate interpolation procedure for obtaining a three-dimensional spatial distribution of three-component velocity, using randomly measured ADCP observation data, was developed in order to extract the complex flow characteristics of actual riverine flow. Turbulent properties can be estimated using a statistical analysis of the data obtained from a fixed point ADCP survey (*Kristensen and Gaynor* [1986]; *Lu and Lueck* [1999]); however, this approach is not suitable for a random survey obtained from ADCPs. In this study, a different approach, namely a method designed to reconstruct detailed and precise mean flow distributions from randomly measured ADCP data, is proposed.

2. The reconstruction of the three-dimensional velocity field using randomly-measured ADCP data

In ADCP surveys within a river, the boat is navigated and measured points are consecutively displaced according to the navigation of the boat; and the velocity under the boat's trajectory is measured. When attempting to measure the entire focused reach of a river, precisely maneuvering a boat on a planned course is difficult, since the boat's trajectory is strongly impacted by the turbulence and surface wave. Therefore, the trajectory of the measurement should be assumed to be irregular. An irregular path spans the target area of interest for moving boat ADCP measurements, and intersects at various points, forming an irregular network. In this study, a procedure for data processing using a measured raw ADCP velocity vector, in order to obtain an accurate velocity distribution, is proposed. A block diagram of the developed procedure is shown in Fig. 1. The
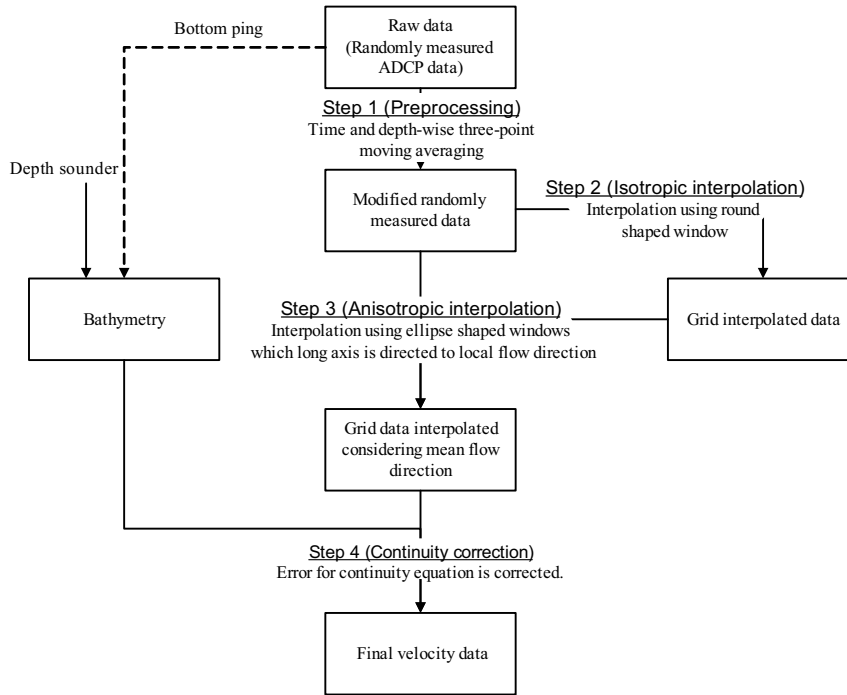
Figure 1. The procedure for the interpolation of ADCP data.

procedure consists of four steps, as outlined below. Step 1 is a pre-process where a moving average with a small averaging window is applied to raw ADCP data in order to reduce spiky noise due to random error and emergent turbulence. In Step 2, a velocity field is applied to the regular (Cartesian) grid by averaging the velocity data from Step 1. In Step 3, the velocity field is applied once more from pre-processed velocity data onto the regular grid. The difference between Steps 2 and 3 is that in Step 3 the averaging window is distorted toward the local flow direction. The direction of local flow is obtained using the flow field processed in Step 2. In this work, Step 3 is called "Anisotropic gridding" and is introduced in order to obtain a precise flow structure without over-smoothing the velocity distribution. The raw ADCP data provides a depthwise distribution of the velocity. The interval in the depthwise direction is an adjustable parameter and is kept constant during the observation set. In Steps 2 and 3, the velocity data at each water depth is treated separately and is conducted individually for each water depth plane. In Step 4, the velocity that was gridded in Step 3 is revised using a continuity correction process in order to reduce the error of the mean velocity field due to macro turbulence, and systematic and random errors. Details for each of the steps shown in Fig. 1 are described in the following section.

2.1. Step 1 (Pre-processing)

In the first step, in order to eliminate small disturbances in the flow and random errors in measurements, a moving average procedure for both the depthwise and temporal directions is applied. The process is partially included in the ping ensemble calculated with the ADCP system. To reduce sharp spiky noise, three-point averaging for all neighboring depth cells is applied to all of the interior components of the velocity (*Dinehart and Burau* [2005a]). The size of the averaging window is twofold the sampling time and depth intervals. Step 1 is designed to be used in case the fluctuation of the raw data is remarkable. However, in the area

and data set, as discussed in Sections 3 and 4, it is revealed that this step has a limited impact on the final result.
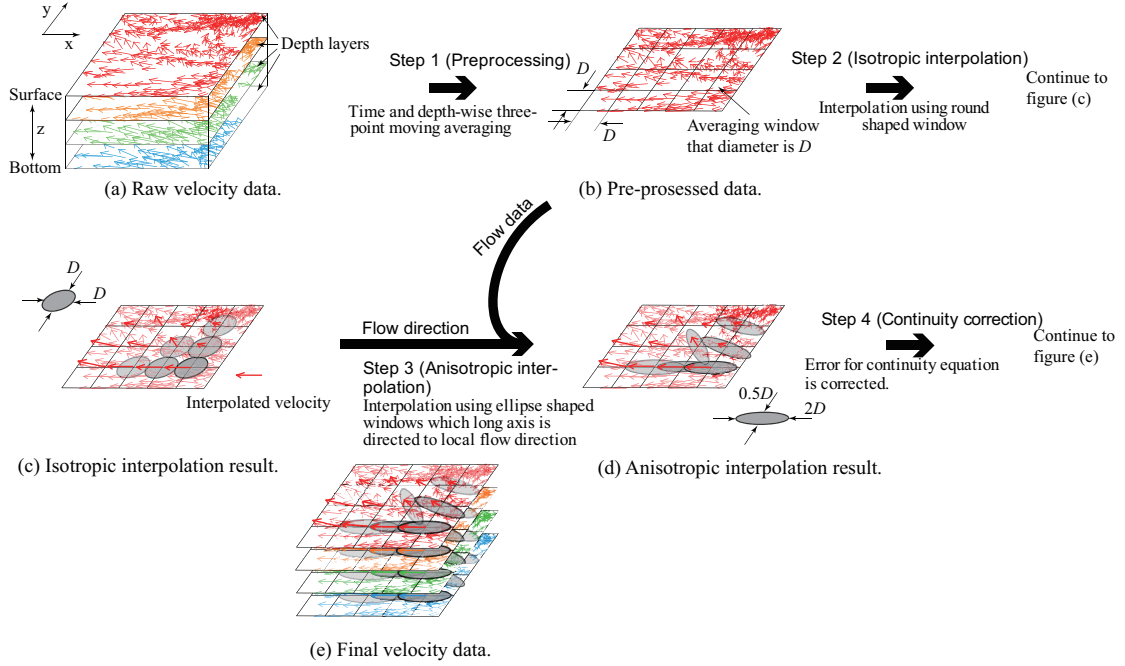
2.2. Step 2 (Isotropic gridding)

In Step 2, a horizontal regular grid system with grid spacing D is configured (Fig. 2b). As shown in Fig. 2c, velocity vectors within a specific cell in the grid are averaged separately in each depth layer. A smaller grid size improves the spatial resolution of the distributed information. However, as the numbers of measured data that are included in each cell becomes smaller, the reliability of the information in each cell becomes lower. Additionally, by using a small grid size, the number of empty cells for raw ADCP values is increased, indicating that the amount of interpolated information is also increased. The sensitivity of grid spacing to the accuracy of the interpolated velocity may be impacted by a relative data density ρ_d, the complexity of the flow, and the magnitude of the velocity fluctuation. Here, the relative data density ρ_d is the ratio of the data point number per the effective grid cell number N_g, as follows:namely

$$\rho_d = \frac{LF}{U_v N_g} \tag{1}$$

where L is the total distance along the measurement route, F is a data sampling frequency, and U_v is the vessel navigation speed. In section 3, the sensitivity of the relative data density to the interpolated velocity will be discussed.

2.3. Step 3 (Anisotropic gridding)

In the third step, velocity averaging along the same streamline aims to precisely extract the mean flow structure and to efficiently remove random components contained in the measured value. In order to achieve this goal, an averaging procedure that considers the horizontal flow direction at each point is conducted. For this step, the velocity data obtained in Step 1 is averaged over an ellipse whose center is located in the middle of the cells of a grid that, as shown

(a) Raw velocity data.

(b) Pre-prosessed data.

(c) Isotropic interpolation result.

(d) Anisotropic interpolation result.

(e) Final velocity data.

**Figure 2.** The scheme of the interpolation procedure.

in Fig. 2d, has a length of $2D$ on the major axis and $0.5D$ on the minor axis. The direction of each ellipse is configured based on the local velocity obtained in Step 2. The size of each ellipse is determined in order to keep the number of data on the same order as those of the averaged cell points that contain raw ADCP data.

Here, since macro turbulent flow is essentially convected along the mean flow direction, the flow structure along the same streamline is assumed to be almost conserved in a closed space. The purpose of taking an average toward flow direction is that we can expect to obtain an accurate mean velocity field by efficiently removing fluctuations contained in the instantaneous data due to instrumental error and the turbulence of the flow. The additional advantage of introducing the streamwise averaging window is that this operation prevents an over-smoothing of the velocity distribution across a shear layer region. Moreover, the trajectory of the random ADCP survey produces a mesh net, and the ratio of each averaging window containing one or more measured data points increases by utilizing the ellipse-shaped averaging window.

The shape of the ellipse is controversial. For simplicity, and in order to focus on establishing a general framework for the new method, the size of the ellipse was fixed as $2D$ by $0.5D$. An adaptation of the ellipse shape, based on the measured density and the flow in velocity and time, is expected to provide a better estimate, but is not discussed in this work.

2.4. Step 4 (Continuity correction)

Thus far, the three-component velocity distribution on a three-dimensional grid has been obtained using procedures from Steps 1 through 3. The steps are a type of averaging procedure in space and time, and are aimed at obtaining a mean velocity field by removing fluctuating components. On the other hand, the measured value not only contains fluctuations due to turbulence and instrumental error but also to systematic errors of the measurement, such as the shifting downward velocity component w surrounding the water's surface (*Dinehart and Burau* [2005b]). Since these systematic error factors cannot be removed with a simple averaging operation, another correction procedure is necessary. Therefore, in Step 4 the velocity distribution correction based on mass conservation is introduced.
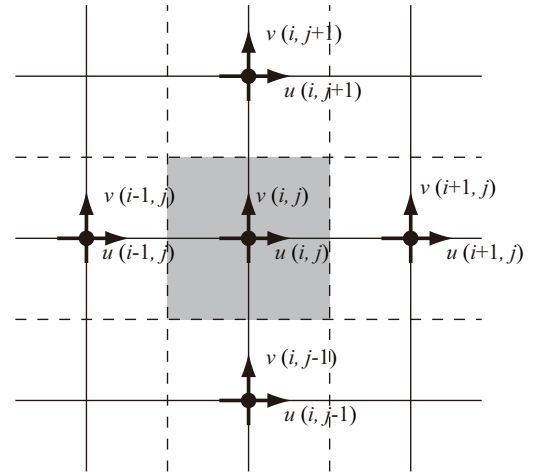
Figure 3. The allocation of the flow parameter used in the continuity correction. The shaded region indicates that the domain representative velocity $u(i,j)$ and $v(i,j)$ correspond.

To achieve the objective of Step 4, a technique used in computational fluid dynamics (CFD) is required. The fractional-step method (*Chorin* [1968]; *Temann* [1969]; *Yanenko* [1971]) is one of the most widely used methods in the CFD field for solving Navier-Stokes and continuity equations. In the fractional-step method, momentum equations without pressure terms are calculated in order to obtain an intermediate velocity distribution; then, the Poisson equation is solved using the intermediate velocity, and, subsequently, the pressure distribution is calculated. Finally, in the next time step, the velocity distribution is obtained by correcting the intermediate velocity distribution using pressure distribution data.

In this study, the velocity distribution obtained in Step 3 is used for calculating the pressure distribution, by using an iterative calculation to solve the Poisson equation. The velocity distribution is then corrected using the pressure dis-

tribution calculated by the Poisson equation. The corrected velocity distribution is expected to contain reduced error with respect to the mass conservation law, when compared with the velocity before the correction. To calculate the pressure distribution, a regular-grid type allocation of flow parameter is utilized (see Fig. 3).

The first step in the correction is to solve the following equation:

$$\nabla^2 p = \frac{\nabla \cdot \boldsymbol{U}}{\alpha} \tag{2}$$

where $\boldsymbol{U} = (u, v, w)$ is the velocity vector, α is a parameter related to time progress, and $\alpha = \frac{\delta t}{\rho}$ is used for an unsteady flow simulation. Zero pressure at the water's surface, and a zero gradient for pressure within the river bed were used for the boundary condition of p. For calculating $\nabla \cdot U$ the pressure weighted velocity interpolation is needed (*Armfield et al.* [2010]) to avoid checker-board instability.

The second step in the correction utilizes the following equation:

$$\boldsymbol{U}^* = \boldsymbol{U} - \alpha \nabla p \tag{3}$$

where $\boldsymbol{U}^*$ is the corrected velocity vector. The mean flow field is a main concern in this study. Therefore, α works only on a portion of the magnitudes of velocity and pressure. In order to estimate pressure quantitatively, α should be specified using a calculation time step from the numerical flow simulation. In the framework of this study, the value of α can be selected arbitrarily.

Since it is impossible to measure the entire spatial distribution of the velocity in an instant while using an ADCP, the spatial velocity distribution does not completely satisfy the continuity for a fluid. However, the aim of the method presented is to obtain the mean velocity field from randomly-measured velocity information. The mean velocity field satisfies the mass conservation law, so the utilization of the continuity correction is rational for obtaining an accurate mean velocity distribution.

2.5. Summary

The proposed procedure is oriented not for obtaining a smoothed velocity field but for removing fluctuations of instantaneous velocity without over-smoothing the velocity distribution near a shear region, by introducing averaging along the advective (streamwise) direction. The continuity correction removes spike-noise and reduces systematic error. The procedure that is introduced in this study is simple but fits the nature of river flow. The applicability of the proposed method is discussed in the following section.

3. The evaluation of the proposed method using model ADCP data

3.1. The numerical flow simulation and ADCP model data

To evaluate the accuracy of the developed method, the unsteady flow data calculated using a three-dimensional flow simulation was utilized. Flow data was calculated using a detached eddy simulation (DES, *Spalart et al.* [1997]). A river confluence flow, whose planform is asymmetrical with a junction angle of approximately 60° (*Rhoads and Sukhodolov* [2001]), was represented by DES (*Miyawaki* [2009]). In Fig. 4, the bathymetry of the confluence presented in the numerical simulation is depicted. Flow conditions for simulated flows were based on the field data shown in Table 1. The calculated flow information, including flow structure and scalar transport, was validated (*Miyawaki* [2009];
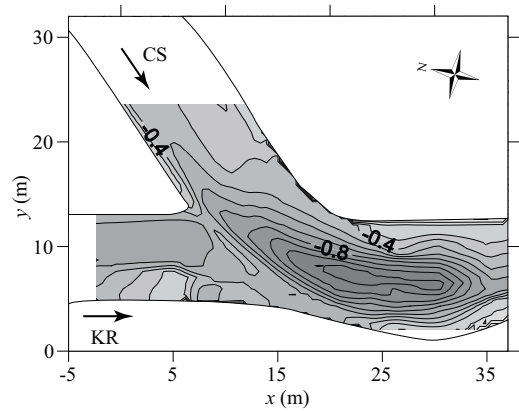
Figure 4. The bathymetry of the numerical simulation channel. Contour lines show the distance from the water's surface at 0.1 m intervals. CS and KR indicate the stream names, the Kaskaskia River and the Copper Slough, respectively.
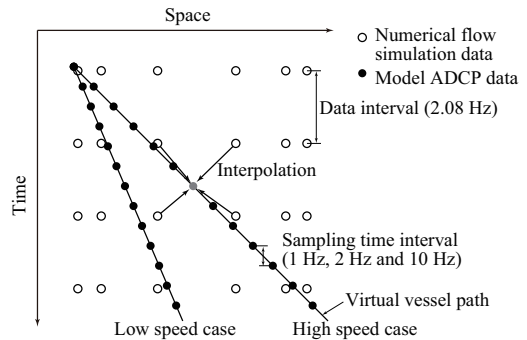
Figure 5. The schematic diagram of the model ADCP interpolation obtained from numerical low simulation data. The actual three dimensional space axis is represented as one dimensional in the figure.

Constantinescu et al. [2011]) by comparing field measured data (*Rhoads and Sukhodolov* [2001]), and we observed that main flow features were reasonably represented by the calculated result. The computational grid was composed using 4.5 million cells (576×288×28 in streamwise, spanwise, and vertical directions). Due to this fine calculation grid, not only macro turbulence but also turbulence with small scales in space and time is clearly and impressively resolved in the turbulence model (*Constantinescu et al.* [2011])

The directions of x, y, and z (and the u, v, and w components) roughly corresponded to the streamwise, spanwise, and vertical directions, respectively.

As shown in Fig. 5, the model of the ADCP data was interpolated from numerical flow data. One hundred instantaneous velocity fields that were stored at an interval of 2.08 Hz (48 seconds in duration) were used to calculate the mean velocity field and to generate the model ADCP data. A dominant frequency for the vortices emerged in the mixing region formed in the confluence of approximately 0.2 Hz, so the stored data resolved 10 snapshots per cycle and contained 10 cycles in total. As shown in Fig. 6, for modeling the randomly-measured ADCP survey, the hypothetical measurement route of the moving ADCP survey was configured. The total distance along the measurement route was 450 m. Throughout this route a three-component local velocity at 0.1 m intervals in the depthwise direction was reconstructed by interpolating the raw velocity data in

Table 1. The hydraulic conditions of the numerical flow simulation *Miyawaki* [2009]; *Rhoads and Sukhodolov* [2001]

Stream	Q (m^3/s)	U (m/s)	ρQU (kg m/s^2)	B (m)	H (m)
Kaskaskia River (KR)	1.41	0.42	597	6.9	0.48
Copper Slough (CS)	1.34	0.46	615	9.0	0.32
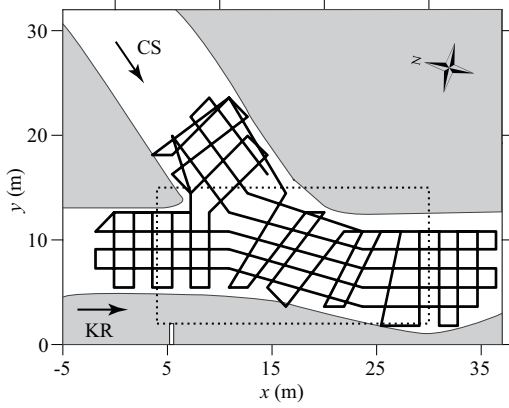
Figure 6. The measurement route of the model ADCP survey. The area indicated inside the dotted rectangle indicates the region for velocity gridding.

Table 2. The parameters utilized in the Kriging interpolation

Range	0.3
Zero value	0.0
Drift	NoDrift
Point selection	Octant
Number of points	8

Table 3. The parameters used in the inverse-distance weighting interpolation

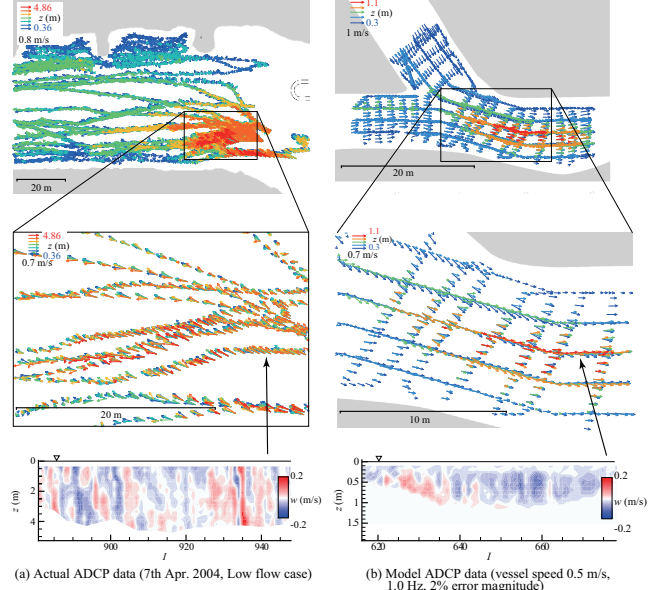| Minimum distance	-
Exponent	3.5
Point selection	Octant
Number of points	8

space and time. The depthwise velocity distribution at the virtual measurement point moving along the measurement route was recorded at 10 Hz. Sampling frequencies of 1.0 and 2.0 Hz were also used to identify the effect of sampling density on the interpolated velocity field. Five different vessel speeds (0.25 m/s, 0.5 m/s, 1.0 m/s, 2.0 m/s, 10 m/s, and 20 m/s) were used to confirm sensitivity to the vessel navigation speed and the total number of velocity data. The vessel speed was kept constant. For a case of navigation speed of 1.0 m/s and a frequency of 2.0 Hz, the total duration for measuring the entire measurement route was 450 seconds, and the total number of measurement points was 900.

To model random error in the actual measurement, a white noise whose standard deviation was 2 % of the local velocity magnitude $|\boldsymbol{U}|$ (*Fugate and Chant* [2005]) was added to the original data. The range of the random error depends both on the measurement configuration and the flow situation, so error magnitudes of 1 and 5 % were also tested in order to identify the sensitivity to the obtained velocity field.

Then, for modeling systematic error in the depthwize velocity component w in the near water surface area (*Kim et al.* [2009]), the following error model was introduced:

$$w'_z = w_z - 0.05 \frac{\tan\left(1.5\left(H - z\right)/H\right)}{\tan\left(1.5|\boldsymbol{U}|\right)} \qquad (4)$$

where w'_z represents the velocity of the model error at a depth of z, H is the depth of water column, and $|\boldsymbol{U}|$ is the

(a) Actual ADCP data (7th Apr. 2004, Low flow case)   (b) Model ADCP data (vessel speed 0.5 m/s, 1.0 Hz, 2% error magnitude)

Figure 7. Comparison of the model and actual ADCP data sets. The upper part depicts vector plots over water depth. The colors of vector corresponds to the water depth of each vector. The left-hand part depicts a data set of ADCP survey measuring a reach of the Uji River. A detailed description of actual ADCP data is described in Section 4. The right-hand part shows model ADCP data prepared in Section 3. The lower part of this figure shows depthwise distributions of vertical velocity component w along the measuring transects (I stands for ping number).

(a) u'_{rms} vs. u (b) v'_{rms} vs. u (c) w'_{rms} vs. u
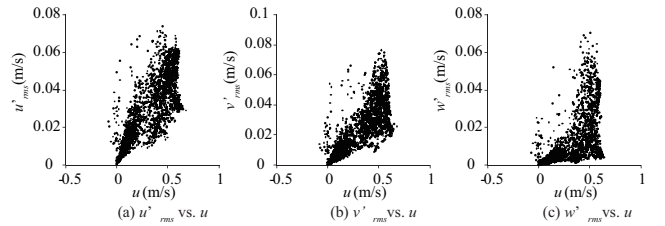
Figure 8. The correlations between the turbulence intensity components and the streamwise velocity magnitude.

velocity magnitude at the focusing point. The error model was based on observational data as reported by *Dinehart and Burau* [2005b] and the values measured by the authors.

Using the method described in Section 2, velocity data along the measuring route was interpolated onto a regular grid where the grid spacing D was 1.0 m. The gridded region was 4.0 m$\leq x \leq$30 m and 2.0 m$\leq y \leq$15 m (shown as a dotted rectangle in Fig. 6). Therefore, the grid cell number in the horizontal plane was $27 \times 14 = 378$. Some of the grid cells were located within the dry bed area, so the number of cells containing open water was 283. In the vertical direc-
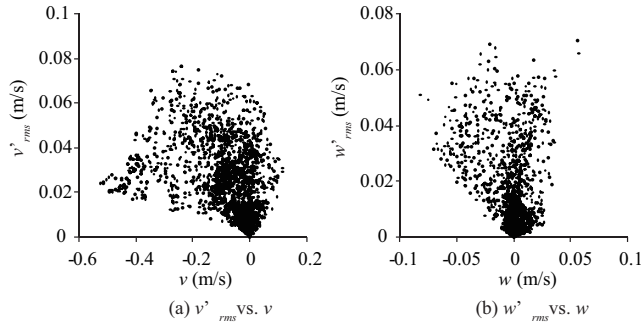
Figure 9. The correlations between the turbulence intensity components and the corresponding velocity magnitude component.

Figure 10. A comparison of estimated and correct values for three velocity components. The estimated velocity components were calculated using the proposed method.

tion, fifteen layers with 0.1 m intervals were configured. The velocity field was interpolated using the method described in Section 2. Fig. 7 compares vector plots of the hypothetical ADCP data set prepared in this section and an actual river flow data measured by moving ADCP survey. Key features of moving ADCP survey, inhomogeneity of measuring point and variation of velocity in horizontal and depthwise directions were represented well in the model ADCP data set. In the depthwise distribution of w component distribution along measuring trajectory shown in the lower part of the Fig. 7, relatively large fluctuation due to turbulence and measurement noise is observed in both the actual and model ADCP results.

As a benchmark, velocity data in the regular grid was interpolated using three-dimensional Kriging applied to ADCP model data (see e.g. *Rennie and Church* [2007]; *Jamieson et al.* [2011] for the Kriging application in the ADCP data interpolation). Parameters used in the Kriging interpolation are listed in Table 2. Additionally, another widely used interpolation method, the inverse distance weighted (IDW), was used to generate the gridded velocity field. The parameters used in the IDW operation are described in Table 3. Both the Kriging and IDW interpolations were conducted using the built-in functions of Tecplot 10, Tecplot Inc. (WA, USA)

As correct velocity data, the mean velocity at each point was calculated by averaging 48 seconds of original CFD data.
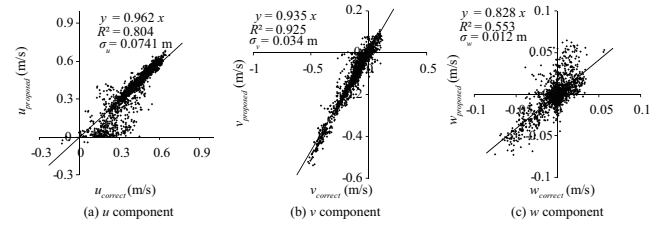
3.2. The results of the validation

In this subsection, performance of the proposed method is discussed. The magnitude of the turbulence intensity is one of the dominant factors that impacts the error of the gridded velocity. The magnitude of the turbulence intensities and their relation to the local mean velocity were confirmed. Then, the error of the velocity components for grid points calculated using the proposed method were quantitatively validated. As a result, the adequacy of velocity distributions calculated using the proposed method, and the Kriging and IDW methods were compared. At the end of this section, the impact of data point density is identified.

3.2.1. Relative turbulence intensity

In advance of a discussion on the performance of the proposed method, the fundamental turbulent characteristic of the flow, as treated in this section, was investigated using a flow data directory calculated from CFD data without errors.

In Fig. 8, correlations between the turbulence intensities and the streamwise velocity component u are shown. In general, the range of turbulence intensity components was increased in proportion to the magnitude of the streamwise velocity. The maximum range was approximately 0.08 m/s and the magnitude of the maximum value of the turbulence intensity was almost identical for the three velocity components.

In Fig. 9, correlations between the turbulence intensities and the corresponding velocity magnitude components are shown. The scattering patterns in Fig. 9 differ from those in Fig. 8. The magnitude of the turbulence intensity is mainly correlated to the streamwise flow structure. The turbulence intensities of the transverse (v) or vertical (w) components are not identical, but are strongly regulated by streamwise flow. Even if the magnitude of the transverse or vertical velocity is small, the corresponding turbulence intensity displays an order of v'_{rms}, such that the relative turbulence intensities ($\frac{v'_{\mathrm{rms}}}{v}$ and $\frac{w'_{\mathrm{rms}}}{w}$) become comparatively large, making it difficult to accurately reconstruct mean velocity components for v, and especially w.

3.2.2. A comparison of point data

In Fig. 10, the correlation between each velocity component corrected and obtained using the proposed method is depicted. The ADCP data modeled here simulated the conditions of data collection. The vessel speed was 1 m/s, the sampling frequency was 10 Hz, and the random error magnitude was 2 %). In the streamwise component u, shown in Fig. 10a, a scatter range of u_{proposed} in the low velocity range ($|u_{\mathrm{correct}}| < 0.4$ m/s) was wider than the range of high velocity. The low velocity area within the streamwise velocity corresponded to an area close to the river bed/bank or to a stagnated area. In these areas, especially near river beds and banks, the spatial gradient of the velocity was large, and caused a comparatively large error. In the mixing zone, the mean streamwise velocity u was over 0.4 m/s, and, as can be seen in Fig. 10a, the scatter in the range range over 0.4 m/s was relatively small. This support that the gradient of mean velocity in the mixing zone was interpolated accurately.

The plot of the transverse component v (Fig. 10b) displayed small scatter (σ_v=0.034 m) and the estimated velocity represented the correct velocity with small systematic errors (the slope of the fitted line was 0.935). For the vertical component w (Fig. 10c), scatter in the plot was comparatively large. Since the relative turbulent intensity $\frac{w'_{\mathrm{rms}}}{w}$ was quite large, a larger velocity estimation error for the w component was observed.

For both the u and v components, the slope of line fitting was close to unity, the determination coefficient was sufficiently large ($R^2 = 0.804$ and $R^2 = 0.934$ for u and v, respectively), and the standard deviation was reasonably small ($\frac{\sigma_u}{u_{95\%}} = 0.12$ and $\frac{\sigma_v}{v_{95\%}} = 0.086$, here e.g. $u_{95\%}$ is the top 95% value of the velocity magnitude.) The results denote that the spatial distribution of u and v, calculated with the proposed method, represents an accurate mean flow structure. For the w component, the determination coefficient was low ($R^2 = 0.553$). Comparatively large scattering

in the low w magnitude area led to the low R^2 value. The relative standard deviation for the w component $\frac{\sigma_w}{w_{95\%}}$ was 0.32 and the slope of the fitting curve was 0.83. Thus, the trend of the w component distribution could be traced, but the w velocity component contained a certain amount of error, as a result of the flow nature, namely the comparatively large relative turbulence intensity in the w component, as confirmed in Section 3.2.1.

3.2.3. Velocity distribution

In Fig. 14, three-dimensional streamlines of the correct velocity field and the velocity fields interpolated using the proposed and Kriging methods are compared. In this figure, the color of each streamline corresponds to the water depth for the initial points of the streamline. In Fig. 14a, in the interface of two stream convergence, streamlines converge at the surface and diverge at the bottom. Also, a descend flow was observed in the interface of the two streams. The flow structure type is generally represented in the results of the proposed method (Fig. 14b) and the Kriging method (Fig. 14c); however, the result obtained using the Kriging method displayed staggering streamlines, indicating that the interpolated velocity field contained a larger degree of fluctuating components due to flow turbulence and measurement noise. In contrast, the result obtained using the proposed method displayed a smooth and consistent configuration of streamlines and better identified the structure depicted in the streamlines generated from the correct velocity field.

In Fig. 15, to confirm vortex tube structure, the second invariant Q (*Hunt et al.* [1988]; *Chacín et al.* [1996]) iso-surfaces, calculated using the velocity field of the correct value and the two interpolation methods, are compared. The second invariant Q was calculated as follows:

$$
\begin{aligned}
Q &\equiv \frac{1}{2}\left((u_{i,i})^2 - u_{i,j}u_{j,i}\right) = -\frac{1}{2}u_{i,j}u_{j,i} \\
&= \frac{1}{2}\left(\Omega_{i,j}\Omega_{i,j} - S_{i,j}S_{i,j}\right)
\end{aligned}
\tag{5}
$$

where $u_{i,j} = \frac{\partial u_i}{\partial x_j}$ and $\Omega_{i,j} = \frac{1}{2}\left(\frac{\partial u_i}{\partial x_j} - \frac{\partial u_j}{\partial x_i}\right)$ $S_{i,j} = \frac{1}{2}\left(\frac{\partial u_i}{\partial x_j} + \frac{\partial u_j}{\partial x_i}\right)$. As shown in equation 5, Q is a subtraction of the shear S from the sum of the rotational and shear motion Ω, so rigid rotation is predominant in the region of $Q > 0$ and shear motion is distinguished in the region of $Q < 0$. In Fig. 15a, the $Q = -0.015$ s^{-2} iso-surface (indicated as a blue surface) was observed along the mixing layer between the two ongoing streams. Along the mixing layer, two rotational flow regions (streamwise-oriented vortices) and $Q = 0.075$ s^{-2}, shown as a red surface, were confirmed. *Miyawaki et al.* [2010] reported that the pair of the flow rotating in the inverse direction exists and is located on both sides of the mixing layer. The Q iso-surfaces, based on the velocity field obtained using the proposed method (Fig. 15b), revealed a similar flow structure, namely for the shear flow observed along the mixing layer and the pair of streamwise-oriented vortices abutting the shear region, even though the distribution in Fig. 15b was slightly obscured as compared with that of Fig. 15a. The velocity field obtained using the Kriging interpolation contained still more error. As shown in Fig. 15c, due to this error it is quite difficult to identify the flow structure using the Q iso-surfaces, since Q is calculated based on the velocity distribution and the low accuracy of the velocity obtained from Kriging veils of the flow structures of the mixing layer and the pair of vortex tubes. In summary, the structures of flow through complex bathymetry, as observed in the corrected data, can be represented clearer when using the proposed method as compared to the Kriging method.
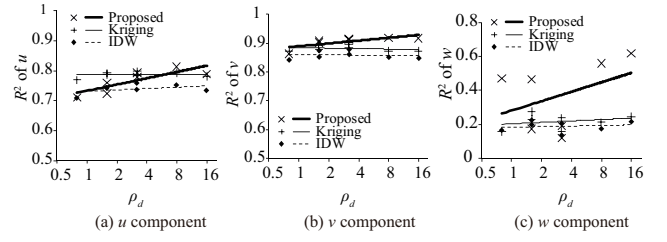
Figure 11. The relationship between the determination coefficient and the data point density for three velocity components. Symbols indicate data points and curves represent exponential fitting curves.
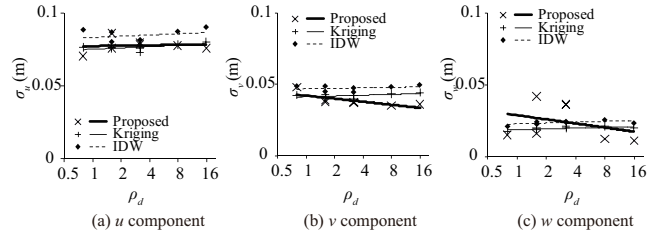
Figure 12. The relationship between the standard deviation and the data point density for three velocity components. Symbols indicate data points and curves represent the exponential fit.
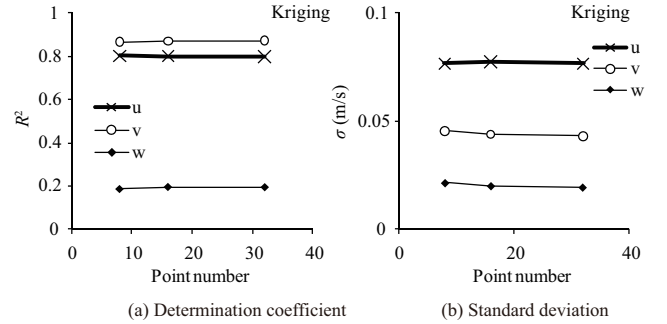

Figure 13. The sensitivity of the point number to estimations of accuracy in the Kriging method for the 0.5 m/s vessel speed case.

3.2.4. The effects of data point density on interpolated velocity

In Figs 11 to 12, the impact of data point density ρ_d (see equation 1) and interpolation methods on the accuracy of the interpolated velocity components are compared. The vessel navigation route is shown in Fig. 6. The total distance was $L = 450$ m. The vessel navigation speed in the range from U_v=0.5 m/s to 20 m/s was tested; and the sampling frequency was set as F=1.0 Hz, 2.0 Hz, and 10 Hz. The total grid cell number in the horizontal plain was 392, including ($N_g =$) 283 water body grid cells.

In Fig. 11, the relationship between the determination coefficient R^2 and the data point density ρ_d is compared for the three velocity components. For the v and w components, R^2's for the proposed method have a larger value as compared with R^2's obtained using the Kriging and IDW methods for the same data point density. Exceptions were
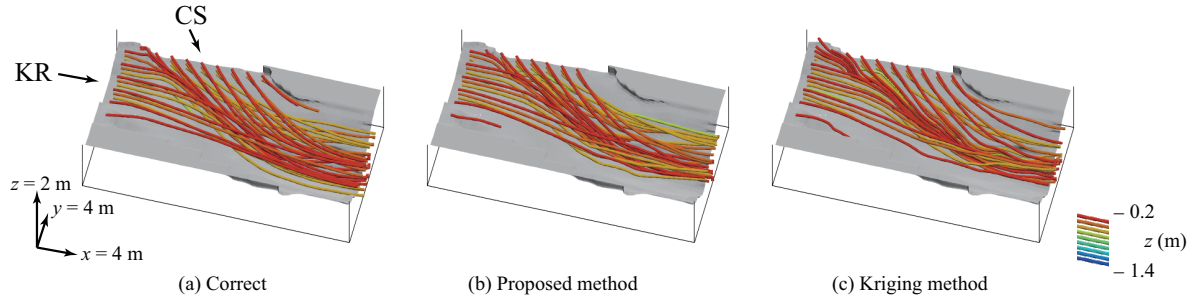
Figure 14. The comparison of streamlines for the corrected velocity field and the interpolated values. The gray surface represents the bathymetry. The vertical and horizontal dimensions are not shown to scale. The colors of the streamlines represent the depths of the starting points for each streamline; red, orange, and yellow represent shallow, intermediate, and deep water levels, respectively.
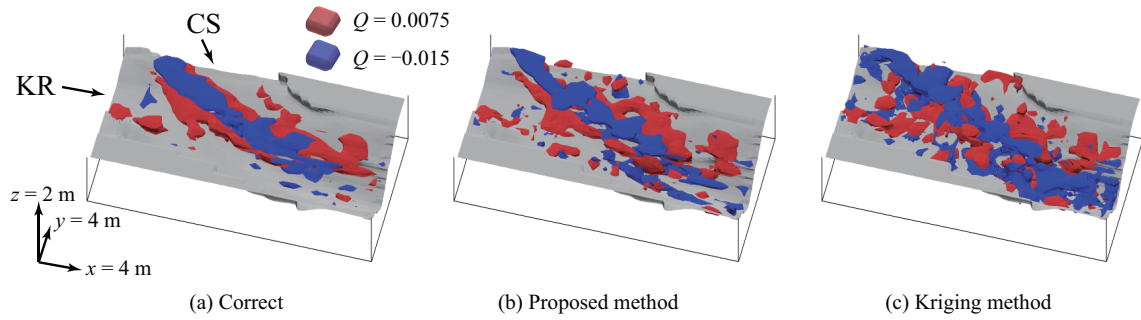
Figure 15. The comparison of the second invariant Q iso-surfaces calculated from the correct velocity field and the interpolated values.
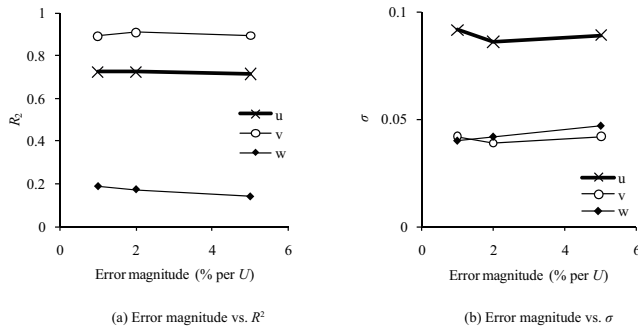
Figure 16. The sensitivity of the error magnitude on the determination coefficient and the standard deviation error for three velocity components interpolated using the proposed method. The vessel navigation speed was 1.0 m/s and the sampling frequency was 1.0 Hz.

observed for the u and w components in the range of low point density. In general, R^2's increased with an increase in data point density in the proposed method; however, the R^2's of the Kriging and IDW methods were kept within a constant range even though the density was increased.

In Fig. 12, the relationship between the standard deviation σ of the three velocity components and data point density is compared. The σ for the u component of the proposed method maintained a specific range but declined for the v and w components with increments for data point density. On the other hand, the σ's for the Kriging and IDW methods slightly inclined in three velocity components, indicating that the Kriging and IDW methods are robust but that the error range is not reduced proportional to an increase in data point density. For the concept of random ADCP measurements, the data points were aligned on a specific route,

so the measuring locations were strongly biased in space and may deteriorate the accuracy of the estimated velocity obtained from methods based on distance weighted averaging in cases of high data point density.
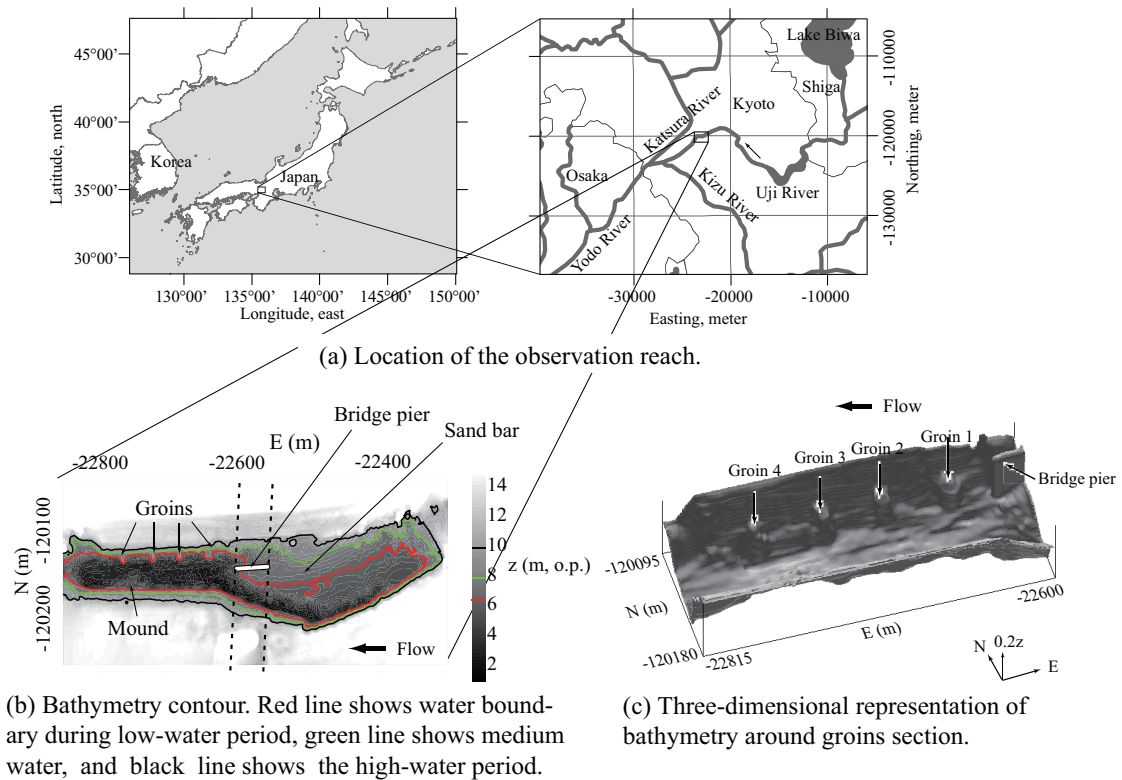
In Fig. 13, a number of the data points used for interpolations in the Kriging method (see Table 2) were changed to 8, 16, and 32 for the model ADCP data (where the vessel speed was 0.5 m/s and the sampling rate was 10 Hz). However, both the determination coefficient and the standard deviation for the three velocity components was keep almost constant. The results suggest that Kriging is a method that is rather insensitive to data point density. However, Kriging is not suited for estimating the velocity distributions of data sets containing a large number of strongly spatially-biased velocity data.

3.2.5. Effects of random noise on the accuracy of interpolated velocity components

In Fig 16, the determination coefficients and the standard deviation errors for the three interpolated velocity components with different error magnitudes are compared. As shown in the figure, the accuracy of the interpolated velocity components was insensitive to additional error, with magnitudes in the range from 1 to 5 %, relative to the magnitude of the local velocity. The result suggests the error depicted in Fig 16 is due to the turbulence resolved in the CFD model and the random noise is substantially removed by the proposed method.

3.3. Summary

In conclusion, the proposed method shows superior accuracy, as compared with Kriging and IDW. For cases of sufficient data point density it is possible to reconstruct the flow data. However, the proposed method shows relatively poor performance for cases of low data point density. For a case where the data point density ρ_d is larger than three, the determination coefficient and the standard deviation error of

(a) Location of the observation reach.

(b) Bathymetry contour. Red line shows water boundary during low-water period, green line shows medium water, and black line shows the high-water period.

(c) Three-dimensional representation of bathymetry around groins section.

Figure 17. Topographical information. The digital elevation model, shown here, was created from both terrestrial LiDAR measurements (for above-water ground) and ADCP measurements (for under-water bathymetry) during low-flow periods.

the velocity obtained using the proposed method displayed an advantage over the Kriging and IDW methods, especially for the v and w components. In this section, we confirmed that the Kriging and IDW methods are comparatively insensitive to data point density, so it is reasonable to apply Kriging or IDW for random data with lower data density. However, in cases of high data density, the IDW and Kriging methods provided lower accuracy, as compared with the proposed method. Random ADCP data has a continuous pathway. Large scale turbulence has a larger magnitude of variation and its time-scale is larger than the sampling rate of an ADCP survey. Neighboring data points tend to be affected by identical large-scale fluctuations. Therefore, neighboring data points have a tendency to display similar bias from the mean velocity components. Not only the IDW method, but also the Kriging method, failed to show a strong bias for location and velocity magnitude. As a result, the Kriging and IDW methods are not suitable for processing high density random ADCP data.

4. The application to actual river flow

4.1. Study site

A reach of the Uji River (Fig. 17) was investigated using a boat-mounted ADCP. The device used for this work was a Workhorse Sentinel ADCP, Teledyne RD Instruments (CA, USA). Table 5 summarizes three observation cases that are compared in this section and in Table 4. Major configuration parameters for ADCP measurements are also listed. The data point density was 5.3 to 11.6 points per grid cell. In this reach, four spur-dikes, a bridge pier, and the meandering of the low-flow channel caused by alternative sand bars generated a complex flow; and the structure of the flow drastically changed depending on the flow rate (*Fujita et al.*

Table 4. ADCP configurations.

Ping interval (s)	1.10 to 1.20
Bin height (m)	0.25
Ping par ensemble	1
Water mode	12
Number of sub-pings	20
Bottom ref	Bottom track

[2003]; *Muto* [2004]; *Muto et al.* [2005]). The level of the spur-dikes crown was approximately 7.8 m. Differences in flow structure, in relation to different flow conditions, are discussed using the velocity field obtained with the proposed method.

4.2. Stream lines and flow structure

In Fig. 18, streamlines for the three cases are compared. For the low flow case, the main flow curves on the left side in the upstream area are depicted in Fig. 18a. As shown for the general view of the site (Fig. 17b), a sand bar was found surrounding the bridge pier, and was emerged in cases of low and medium flow periods. As a result, the main flow for these flow conditions meandered along the topography of the bed so that the main flow curved to the left. Four spur dikes also emerged and circulatory flows were formed between groins two and three, and between groins three and four. In the area between the bridge pier and groin two, a comprehensive stagnation zone was formed.

For the medium water stage case, as shown in Fig. 18b, the top of the spur dikes were submerged such that the circulatory flow in the dike section almost disappeared and a leaving flow from the right bank was observed in the surface flow. Circulatory flow was observed in the area behind the bridge pier. In the case of a low flow condition, the flow in this area stagnated. In the case of a medium flow condition, the main flow still meandered along the bed form, but

Table 5. Observation cases.

	Case 1	Case 2	Case 3
Observation date	7th Apr. 2004	26th Aug. 2004	22nd May 2004
Water stage (m in Osaka pale)	6.41	8.43	11.27
Condition of groins	Non submerged	Submerged	Submerged
Flow rate (m^3/s)	70	329	780
Overall mean velocity U (m/s)	0.51	1.23	1.67
Representative water depth H (m)	5.36	7.16	9.41
Data point number	4551	5342	2735
Number of water body grid cell	407	459	516

(a) Case 1   (b) Case 2   (c) Case 3
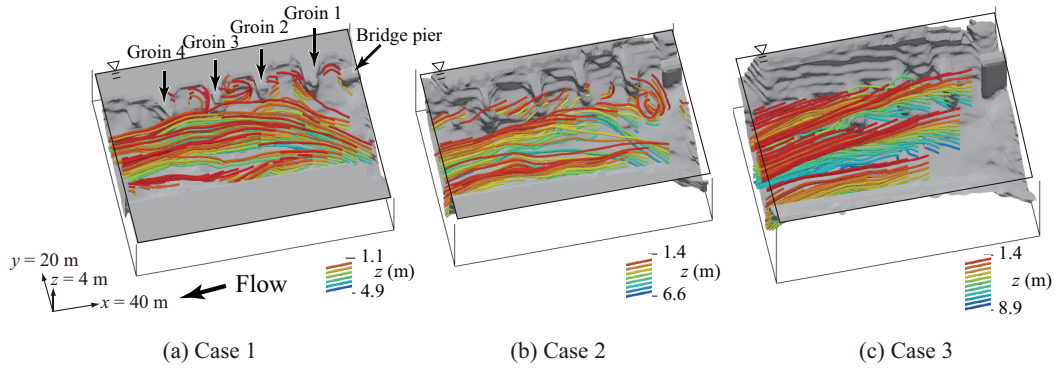
Figure 18. A comparison of the streamlines of the velocity field for different water stages. The gray surface represents the bathymetry. The vertical and horizontal dimensions are not shown to scale. The colors of the streamlines represent the depths of the starting points for each streamline; red, green, and blue represent shallow, intermediate, and deep water levels, respectively.

(a) Proposed   (b) Kriging   (c) IDW
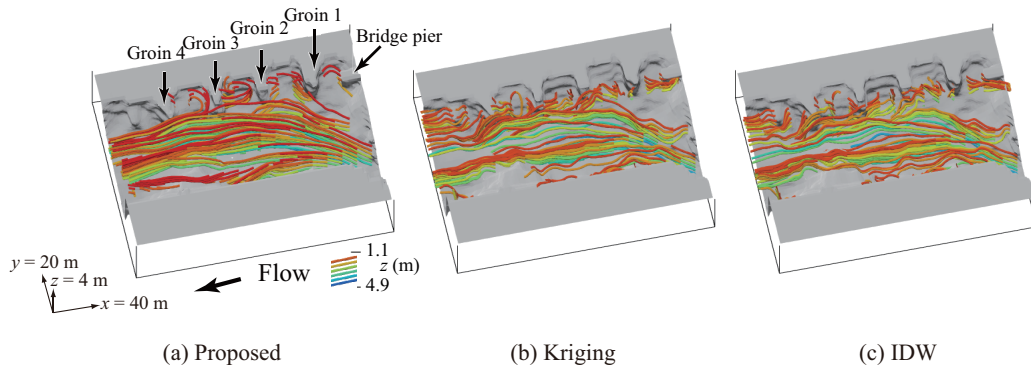
Figure 19. A comparison of the streamlines of the velocity field interpolated using different methods. The gray surface represents the bathymetry. The vertical and horizontal dimensions are not shown to scale. The colors of the streamlines represent the depths of the starting points for each streamline; red, orange, and green represent shallow, intermediate, and deep water levels, respectively.

the shear force between the main flow and the stagnate flow increased, and the stagnate area began to rotate clockwise horizontally.

For the high water stage, as shown in Fig. 18c, surface water flow was nearly parallel with the river bank. On the other hand, the bottom flow in the main stream area curved along the bed from and turned to the left just as the low flow case. Near the right bank, the bottom flow overflowed the groins and the horizontal circulation between the dikes disappeared.

4.3. A comparison of streamlines processed using the three methods

In Fig. 19, the streamlines of the velocity fields for the low flow case, obtained using the proposed Kriging and IDW methods, are compared. The parameters utilized for the Kriging and IDW methods are identical to those used in

Section 3 (see Tables 2 and 3). Results obtained using the Kriging and IDW methods show unrealistically disturbed streamline patterns. The result obtained using the proposed method shows a smooth and consistent configuration for streamlines in both the main flow region and the area between groins. By using the proposed method, the magnitudes of the fluctuating components of the raw ADCP data are substantially reduced. Therefore, as shown in Fig. 19a, essential structures of actual river flow through complex bathymetry can be investigated clearly and precisely using the proposed method.

4.4. Distributions of vorticity $\widehat{\Omega_Z}$

Fig. 20 shows the iso-surfaces of the normalized vorticity $\widehat{\Omega_Z} = \Omega_Z L U^{-1}$, where $\Omega_Z = \frac{\partial v}{\partial x} - \frac{\partial u}{\partial y}$, U is the mean velocity shown in Table 5, and $L = 40$ m is the length scale, which is the streamwise distance of adjacent dikes. For Fig. 20a,

(a) Case 1   (b) Case 3
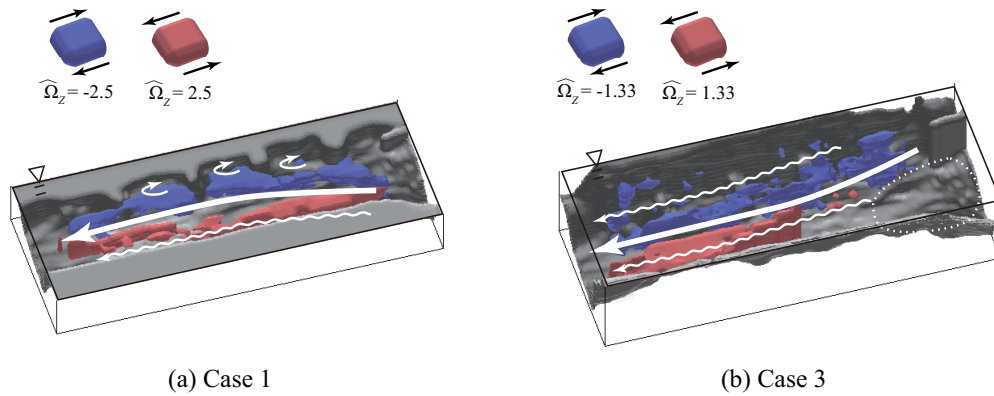
Figure 20. The iso-surface plots of the non-dimensional vorticity $\widehat{\Omega_Z}$. The gray surface represents the bathymetry. The vertical scale is magnified fivefold to clearly represent the flow structure. Note that the white dotted region shown in Case 3 is not part of the observed area. White lines are guides for the eye, and were included to assist with the interpretation of the flow structure.

the low-flow case, a layer of clockwise vorticity (the blue surface), is observed near the right bank. The region represents both the shear-layer region and the circulatory flow formed between the spur-dikes. On the other hand, a counterclockwise vorticity (the red surface) is found near the left bank, indicating that shear flow is formed around the bank. For Fig. 20b, the high-flow case, the thickness of the horizontal vorticity layer is thinner than for Case 1. The difference is related to the role of the shear-layer in the flow for different water stages. For the low water stage, shear is observed close to the river banks. For the high water stage, shear is not formed close to the river bank, but between the main flow and the flow on the flood plain. As shown in Fig. 20, the structure of the flow and its relationship to bathymetry can be investigated visually using the three dimensional contour representation. For drawing three dimensional contours, accurate grid data for the velocity information is essential. In order to calculate the differential quantum, such as the vorticity or the second invariant Q, the requirements for the accuracy of the velocity distribution are very severe. The proposed method adapts to obtain an accurate velocity distribution from moving ADCP data.

5. Conclusion

In this study, the simple but robust interpolation method that takes into account the nature of riverine flow and ADCP measurements is proposed for reconstructing a precise and consistent three-dimensional mean velocity field. The proposed method was confirmed superior accuracy in case density of data point was sufficient, but poor accuracy when data point density was insufficient. Kriging and IDW methods displayed a weak dependency for data point density, so it is a reasonable to use Kriging and IDW for poor density random data. For a condition of sufficient data density these methods provided a lower accuracy as compared to the proposed method. Flow structures at the river reach for spur dikes with different water stages were excluded and the applicability of the proposed method for actual field data was demonstrated.

In this study, grid spacing D was determined in order to assure that 95% of the cells contained at least one raw ADCP data point, and the ellipse shape was fixed at $2D$ by $0.5D$. However, further investigation is needed in order to establish a method for determining the optimum grid size and the ellipse shape. The optimum configuration may be determined by considering the measurement density and the flow scales to be investigated. The optimal procedure for the pre-process (Step 1) leaves much in the way of development. In the place of Steps 2 and 3, IDW or Kriging can be utilized. Therefore, it is also worthy to investigate the performance of these combined methods.

References

Armfield, S., N. Williamson, M. Kirkpatrick, and R. Street, A divergence free fractional step method for the navier-stokes equations on non-staggered grids, *Australian & New Zealand Industrial and Applied Mathematics Journal*, *51*, 654–667, 2010.

Blanckaert, K., and H. J. D. Vriend, Secondary flow in sharp open-channel bends, *J. Fluid Mech.*, *498*, 353–380, 2004.

Callede, J., P. Kosuth, J.-L. Guyot, and V. S. Guimarães, Discharge determination by Acoustic Doppler Current Profilers (ADCP): a moving bottom error correction method and its application on the River Amazon at óbidos, *Hydrological sciences*, *45*, 911–924, 2000.

Chacín, J. M., B. J. Cantwell, and S. J. Kline, Study of turbulent boundary layer structure using the invariants of the velocity gradient tensor, *Experimental Thermal and Fluid Science*, *13*, 308–317, 1996.

Chorin, A. J., Numerical solution of the Navier-Stokes equations, *Math. Comput.*, *22*, 745–762, 1968.

Constantinescu, S., G., Miyawaki, B. Rhoads, A. Sukhodolov, and G. Kirkil, Structure of turbulent flow at a river confluence with momentum and velocity ratios close to 1: Insight provided by an eddy-resolving numerical simulation, *Water Resources Research*, *47*, W05,507, 2011.

Dinehart, R. L., Spatial analysis of ADCP data in streams, in *Proceedings of the federal interagency sediment monitoring instrument and analysis research workshop*, Arizona, USA, 2003.

Dinehart, R. L., and J. R. Burau, Repeated surveys by acoustic Doppler current profiler for flow and sediment dynamics in a tidal river, *Journal of Hydrology*, *314*, 1–21, 2005a.

Dinehart, R. L., and J. R. Burau, Averaged indicators of secondary flow in repeated acoustic Doppler current profiler crossings of bends, *Water Resources Research*, *41*, W09,405, 2005b.

Fugate, D. C., and R. J. Chant, Near-bottom shear stresses in a small, highly stratified estuary, *Journal of geophysical research*, *110*, C03,022, 2005.

Fujita, I., Y. Muto, Y. Shimadu, and R. T. an Shiro Aya, Velocity measurements around non-submerged and submerged spur dykes by means of Large-Scale Particle Image Velocimetry, in *Proc. of XXX IAHR Congress*, pp. 409–415, IAHR, IAHR, 2003.

Hunt, J., A. Wray, and P. Moin, Eddies, stream, and convergence zones in turbulent flows, *Center for Turbulence Research Report, CTR–S88*, 193, 1988.

Ishii, H., Systematic errors and corrections of current velocity measured by shipmounted three-beam type ADCP, *Report of hydrographic and oceanographic researches*, *42*, 61–87, in Japanese, 2006.

Jamieson, E., C. Rennie, R. Jacobson, and R. Townsend, 3-d flow and scour near a submerged wing dike: Adcp measurements on the missouri river, *Water Resources Research*, *47*, W07,544, 2011.

Joyce, T., On in situ " calibration"of shipboard ADCPs, *J. Atmos. Oceanic Tech.*, *6*, 169–172, 1989.

Kaneko, A., and T. Ito, Prevalence of ADCP and the associated progress of oceanography, *Oceanography in Japan, Oceanographic Society of Japan*, *3*, 359–372, 1994.

Kim, D., T. Tokyay, M. Muste, G. Constantinescu, and J. A. Gonzales-Castro, An experimental and numerical investigation of near-transducer errors in ADCP measurements, in *Proceedings of 33rd IAHR Congress*, pp. 3542–3550, IAHR, Vancouver, Canada, 2009.

Kristensen, L., and J. E. Gaynor, Errors in second moments estimated from monostatic Doppler sodar winds. part I: Theoretical description, *Journal of Atomospheric and Oceanic Technology*, *3*, 523–528, 1986.

Lu, Y., and R. G. Lueck, Using a broadband ADCP in a tidal channel. part II: Turbulence, *Journal of Atomospheric and Oceanic Technology*, *16*, 1568–1579, 1999.

Miyawaki, S., Numerical investigation of three-dimensional scalar transport at a river confluence, in *Proceedings of 33rd IAHR Congress*, pp. 4814–4821, IAHR, Vancouver, Canada, 2009.

Miyawaki, S., G. Constantinescu, B. Rhoads, and A. Sukhodolov, Changes in three-dimensional flow structure at a river confluence with changes in momentum ratio, in *River Flow 2010*, pp. 225–232, Braunschweig, Germany, 2010.

Muste, M., K. Yu, T. Pratt, and D. Abraham, Practical aspect of ADCP data use for quantification of mean river flow characteristics; Part II: Fixed-vessel measurements, *Flow measurement and instrumentation*, *15*, 17–28, 2004a.

Muste, M., K. Yu, and M. Spasojevic, Practical aspect of ADCP data use for quantification of mean river flow characteristics; Part I: Moving-vessel measurements, *Flow measurement and instrumentation*, *15*, 1–16, 2004b.

Muto, Y., River flow measurements by means of a broadband ADCP, *Annuals of Disas. Prev. Res. Inst., Kyoto Univ.*, *47/B*, 571–580, in Japanese, 2004.

Muto, Y., and Y. Baba, Secondary flow measurements in a river by a boat-mounted ADCP, *Annual Journal of Hydraulic Engineering, Japan Society of Civil Engineers*, *52*, 925–930, in Japanese, 2008.

Muto, Y., Y. Baba, and H. Nakagawa, Velocity measurements in a straight river with a series of groynes by a ship-mounted around ADCP, in *Proc. of XXXI IAHR Congress*, pp. 455–465, IAHR, IAHR, 2005.

Nystrom, E. A., K. A. Oberg, and C. R. Rehmann, Measurements of turbulence with acoustic Doppler current profilers – source of error and laboratory results, in *Proceedings of Hydraulic Measurements and Experimental Methods Conference 2002*, ASCE, Colorado, USA, 2002.

Ohmori, T., Y. Shimizu, and N. Muneta, Measurement of density current in river bend with ADCP, *Annual Journal of Hydraulic Engineering, Japan Society of Civil Engineers*, *41*, 1035–1040, in Japanese, 1997.

Pollard, R., and J. Read, A method for calibrating shipmounted acoustic doppler profilers and the limitations of gyro compasses, *J. Atmos. Oceanic Tech.*, *6*, 859–865, 1989.

Rennie, C. D., and M. Church, ADCP shear stress and bedload transport in a large wandering gravel-bed river, in *Proceedings of 32nd IAHR Congress*, IAHR, Venice, Italy, 2007.

Rhoads, B. L., and A. N. Sukhodolov, Field investigation of three-dimensional flow structure at stream confluences: 1. thermal mixing and time-averaged velocities, *Water Resources Research*, *37*, 2393–2410, 2001.

Spalart, P., W. Jou, M. Strelets, and S. Allmaras, Comments of feasibility of les for wings, and on a hybrid RANS/LES approach, in *International Conference on DNS/LES*, Ruston, Louisiana, 1997.

Stone, M. C., and R. H. Hotchkiss, Evaluating velocity measurement techniques in shallow streams, *Journal of Hydraulic Research*, *45*, 1–16, 2007.

Temann, R., Sur l'approximation de la solution des équations de Navier-Stokes par la méthode de pas fractionaires (i), *Arch. Rac. Mech. Anal.*, *32*, 135–153, 1969.

Tsubaki, R., and I. Fujita, Interpolation and correction of 3-d velocity distribution from randomly measured adcp data, in *Hydraulic Measurements & Experimental Methods Conference*, Lake Placid, NY, 2007.

Yanenko, N. N., *The method of Fractional-steps*, Springer, Berlin, 1971.

R. Tsubaki, Department of Civil and Environmental Engineering, Hiroshima University 1-4-1 Kagamiyama, Higashi-hiroshima, Hiroshima 739-8527 JAPAN. (rtsubaki@hiroshima-u.ac.jp)

Y. Kawahara, Department of Civil and Environmental Engineering, Hiroshima University 1-4-1 Kagamiyama, Higashi-hiroshima, Hiroshima 739-8527 JAPAN.

Y. Muto, Department of Civil and Environmental Engineering, The University of Tokushima, 2-24 Shinkura, Tokushima 770-8501, Japan

I. Fujita, Department of Civil Engineering, Kobe University, 1-1 Rokkodai, Nada, Kobe 657-8501, Japan